Applied Catalysis B: Environmental 147 (2014) 897–903

Contents lists available at ScienceDirect

Applied Catalysis B: Environmental

journal homepage: www.elsevier.com/locate/apcatb

Tungsten nitride decorated carbon nanotubes hybrid as efficient catalyst supports for oxygen reduction reaction

Shengyu Jing[a], Lin Luo[b], Shibin Yin[b,*], Fei Huang[b], You Jia[c], Yi Wei[c], Zhihua Sun[c,**], Yuemin Zhao[c]

[a] School of Information and Electrical Engineering, China University of Mining and Technology, Xuzhou 221116, Jiangsu, China
[b] Low Carbon Energy Institute, China University of Mining and Technology, Xuzhou 221116, Jiangsu, China
[c] School of Chemical Engineering and Technology, China University of Mining and Technology, Xuzhou 221116, Jiangsu, China

ARTICLE INFO

Article history:
Received 30 July 2013
Received in revised form 10 October 2013
Accepted 12 October 2013
Available online 18 October 2013

Keywords:
Fuel cell
Tungsten nitride
Catalyst
Oxygen reduction reaction
Stability

ABSTRACT

Catalysts for oxygen reduction reaction (ORR) are crucial for the commercialization of proton exchange membrane fuel cells. In this work, nanocrystal tungsten nitride decorated carbon nanotubes hybrid (WN/CNTs-M) introduced as Pt catalyst supports (Pt-WN/CNTs-M) is reported for the first time. X-ray diffraction (XRD), transmission electron microscopy (TEM) and X-ray photoelectron spectroscopy (XPS) measurements are adopted to investigate the physicochemical properties of the prepared catalysts. Cyclic voltammetry and rotating disk electrode techniques are employed to study their corresponding electrocatalytic properties. The results demonstrate that the prepared Pt-WN/CNTs-M catalysts exhibit significantly improved activity toward ORR in acid aqueous solutions, which also display better stability in comparison with the other catalysts in the present study. The reason could be predominantly ascribed to the synergistic effect between tungsten nitride and Pt in the Pt-WN/CNTs-M catalysts and the nitrogen-doping effect of carbon nanotubes with ammonia. The tungsten nitride decorated carbon nanotubes hybrid might be a promising alternative for low-Pt or non-Pt catalysts for oxygen reduction.

1. Introduction

Increasing energy demands have stimulated intense research on alternative energy conversion technology [1–5]. Proton exchange membrane fuel cells (PEMFCs) have advantages in efficiency and environmental benignity for hydrogen and oxygen conversion, but their commercialization is hindered by the high cost and poor stability of catalysts [6,7]. Especially, the catalysts for oxygen reduction reaction (ORR) is critical for PEMFCs [8], for the sluggish oxygen reduction on the cathode will restrict cell's performance. Although tremendous efforts have been made [9–12], further reductions through the development of more activity and stable catalysts is still a great challenge. Till now, the Pt or Pt based catalysts are widely used with desirable performance in PEMFCs due to their relatively high activity and stability. However, Pt is rare in the earth, therefore, great efforts are focused on reducing the use of Pt or improving its performance and developing alternatively low-Pt of non-Pt catalysts.

Transition metal carbides, especially tungsten carbides based materials as novel supports have been widely investigated owing to their special chemical and/or electrochemical activities for various reactions [13–16], which are employed as catalyst supports for PEMFCs [17–20] and demonstrate a synergistic effect with Pt, Pd and other metallic particles. Transition metal nitrides display the similar structures and physicochemical properties to their metal carbides [21], which exhibit catalytic advantages over their metal carbides in activity, selectivity, and resistance to poisoning. Mazza and co-workers [22] found that TiN exhibits activity for ORR in alkaline solutions, for the significant electronegativity difference between Ti and N atoms, there are basic and/or acid sites generated which are favorable for ORR. Zhong and co-authors [23] found that the ORR of molybdenum nitride supported carbon (Mo_2N/C) processes an approximate four-electron pathway in acid solutions and the activity is comparable with Pt/C. Theoretic study [24] revealed that the surface of Mo_2N exposes unsaturated Mo and N atoms and 4-fold-type vacancies, which could change the electron distribution and promote the dissociation and adsorption of oxygen. Ando and co-workers [25] adopted the ammonia-treated carbon-supported cobalt tungsten (Co–W/C) as cathode catalysts for PEMFCs, which display high activity for ORR. Band structure calculations reveal that the active surface structures of cobalt tungsten nitrides consisted of Co–O–Co, which could lower the unoccupied orbital of oxygen atoms close to the Fermi level [26]. According to previously report,

* Corresponding authors. Tel.: +86 516 83883235; fax: +86 516 83883501.
** Corresponding authors. Tel.: +86 516 83590139; fax: +86 516 83590138.
E-mail addresses: shibinyin@126.com (S. Yin), sunzhihua_9633@126.com (Z. Sun).

0926-3373/$ – see front matter. Crown Copyright © 2013 Published by Elsevier B.V. All rights reserved.
http://dx.doi.org/10.1016/j.apcatb.2013.10.026

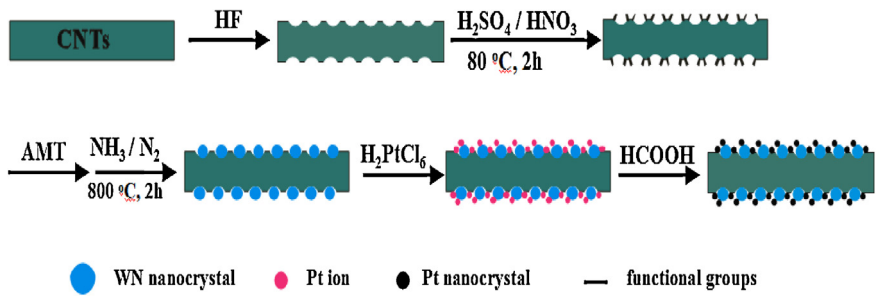

Fig. 1. Schematic illustration of the synthesizing procedures of Pt-WN/CNTs-M.

the tungsten nitride supported Pt displayed better electrocatalytic performance for methanol oxidation than the commonly used Pt/C catalysts [27]. Therefore, the tungsten nitride might be a promising alternative for low-Pt or non-Pt catalysts for oxygen reduction. However, tungsten nitride as catalyst supports for oxygen reduction is rarely reported.

Meanwhile, the carbon nanotubes (CNTs) have also attracted considerable attention as catalyst supports for ORR due to their relatively high electroconductivity, structure stability and corrosion resistance in acid and alkaline environments [28,29]. Nevertheless, due to their almost perfect structure, it is hard for the metallic particles uniformly deposit on their surface. Thereby, the surface modification is necessary to enhance the interactions between the metallic particles and CNTs [30].

Here, in this work, the tungsten nitride decorated carbon nanotubes hybrid is employed as catalyst supports, we are expecting that the performance for oxygen reduction can be improved, and the corresponding chemicophysical properties of the prepared catalysts are investigated. This will be of great interest and significant for the development of cost-effective oxygen reduction catalysts with desirable performance and the synthesized catalysts could also be applied in other fields.

2. Experimental

2.1. Preparation processing

The schematic illustration of the synthesizing process is showed in Fig. 1. Firstly, the CNTs were etched by hydrofluoric acid to make micropores on their surfaces [31]. Then, the H_2SO_4/HNO_3 solutions were employed to make the CNTs hydrophilic and produce some oxygen-contain functional groups on the surface of CNTs [32].

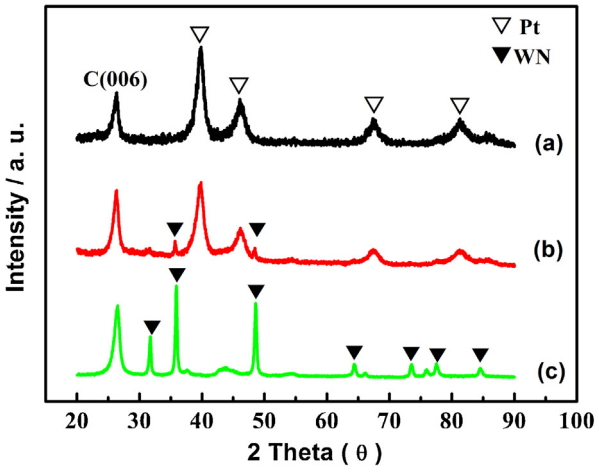

Fig. 2. XRD curves for the prepared samples with a scan rate of 5° min^{-1}. (a) Pt/CNTs-M, (b) Pt-WN/CNTs-M, (c) WN/CNTs-M.

Subsequently, these modified CNTs were adopted as supports to prepare tungsten nitrogen hybrid. Finally, this hybrid was used as supporting material to synthesize catalysts.

2.2. Carbon nanotubes pretreatment

The CNTs with diameters of 10–20 nm and purity of >95% (Shenzhen Nanotech. Co., Ltd., China) were firstly treated by HF solution as follows [31]: 2.0 g CNTs were added into 12.5 g (40 wt%) HF and 37.5 g water under continuous stirring for 6 h at room temperature. After rinsed with deionized water and dried at 100 °C under vacuum for 4 h, they were further treated by H_2SO_4/HNO_3 solutions: 2.0 g pretreated CNTs were mixed with 100.0 mL of a 98% H_2SO_4/65% HNO_3 (3:1, v:v) solutions under constant stirring and refluxed at 80 °C for 2 h. The resulting CNTs were rinsed with deionized water and dried at 100 °C for 4 h, and the obtained samples were denoted as CNTs-M.

2.3. Nanocrystal tungsten nitride synthesis

Tungsten nitride was prepared by temperature-programmed reaction process as follows. The ammonium tungstate ($(NH_4)_6H_2W_{12}O_{40}\cdot xH_2O$, 80.0 mg) was dissolved in 40.0 mL distilled deionized water and 20.0 mL hydrogen peroxide with magnetic stirring. Here, the hydrogen peroxide was employed to dissolve ammonium tungstate. Subsequently, 500.0 mg CNTs-M as supporting material was added into the mixture and stirred until the ink uniformly dispersed. After heated in a draught drying cabinet at 100 °C, they were further reduced in a tube furnace under the mixture atmosphere that composted with 10 mL min^{-1} nitrogen and 10 mL min^{-1} ammonia, with the heating rate of 10 °C min^{-1}, and holding the temperature at 800 °C for 2 h, then it was naturally cooling down to room temperature, the obtained samples were grinded and denoted as WN/CNTs-M.

2.4. Catalysts preparation

The 20 wt% Pt-WN/CNTs-M catalysts were easily and rapidly synthesized by formic acid reduction method [33,34]: 1.25 mL 20.0 mg mL^{-1} chloroplatinic acid as the starting precursor was well mixed with 20.0 mL deionized water in an ultrasonic bath, and then 100.0 mg WN/CNTs-M was added into the mixture. The well-dispersed slurry was obtained with stirring and ultrasonication for 15 min, and then 20.0 mL concentrated formic acid was added into the mixture. Subsequently, after impregnation for several hours till the color turned from yellow to colorless, the resulting black solid samples were centrifuged, washed and dried at 80 °C for 12 h in a vacuum oven. Meanwhile, for comparison, the CNTs-M supported catalysts were prepared by the same way and denoted as Pt/CNTs-M.

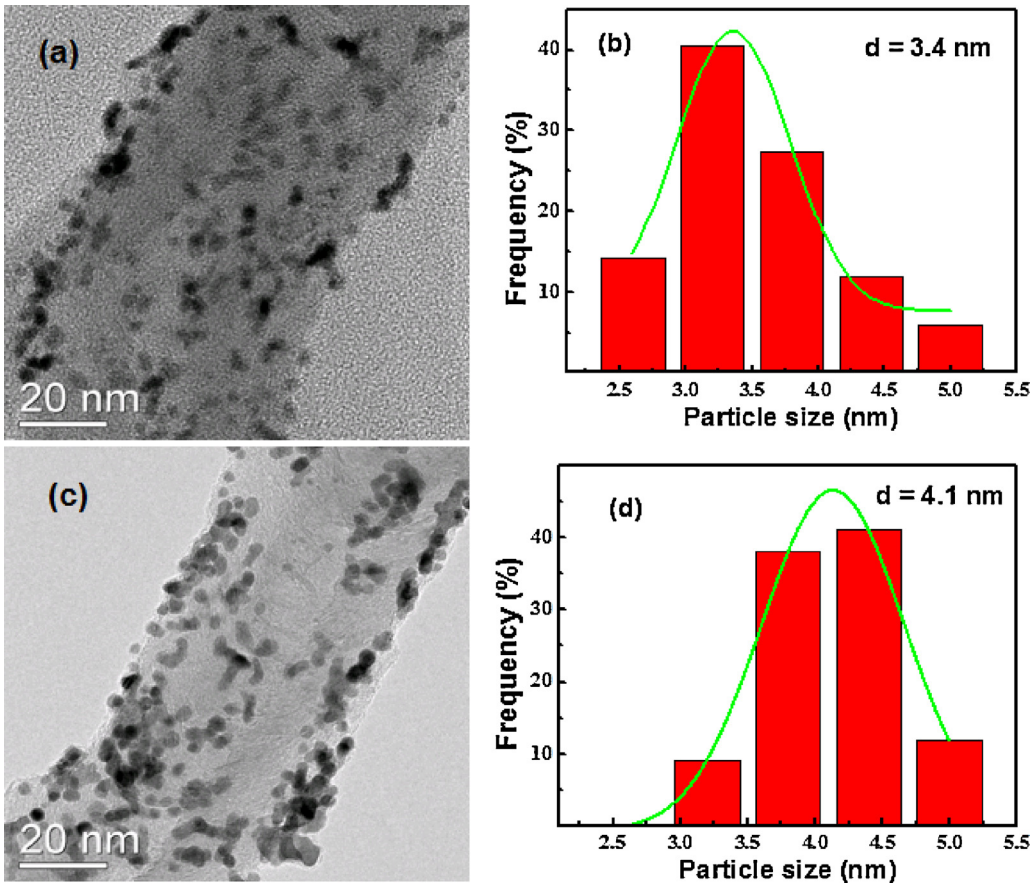

Fig. 3. TEM images of (a) Pt/CNTs-M and (c) Pt-WN/CNTs-M and the corresponding particle size distribution histograms of (b) Pt/CNTs-M and (d) Pt-WN/CNTs-M.

2.5. Catalysts characterization

X-ray powder diffraction (XRD) measurements were carried out on a D8 advance X-ray diffractometer (BRUKER AXS, Germany), using Cu K_a radiation ($\lambda = 0.15406$ nm), and operating at 40 kV and 30 mA. The 2θ angular regions between 20° and 90° were finely scanned at 5° min^{-1}, to obtain the WN and Pt crystal size according to the Scherrer formula [35]. Transmission electron microscopy (TEM) investigations were carried out in a JEOL JEM-2010 (HR) at 200 kV to get information of Pt particle size distribution in the prepared catalysts. The histograms for both catalysts were made by randomly measuring more than 300 particles. The Pt contents were quantified by inductively coupled plasma atomic emission spectroscopy (ICP-AES, PerkinElmer, Germany). X-ray photoelectron spectroscopy (XPS) measurements were obtained by using a ESCALAB 250 Xi (Thermo Fisher Scientific, USA) with the Al X-ray source operated at 150 W. Survey spectra were collected at pass energy (PE) of 100.0 eV over the binding energy range 0–1350 eV.

All electrochemical measurements were conducted on bipotentiostats WD-20 BASIC (Pine, USA) in a thermostatically-controlled standard three-electrode cell at 25 °C, adopting a platinum foil as counter electrode. A saturated calomel electrode (SCE) employed as reference electrode and calibrated against a reversible hydrogen electrode (RHE) as follows: the SCE and platinum foil were placed in 0.1 mol L^{-1} $HClO_4$ aqueous solutions together, and the platinum foil was bubbled with high-pure hydrogen gas, the voltage difference between SCE and platinum foil was measured by multimeter and recorded as RHE. A glass carbon (GC) disk electrode with diameter of 5.0 mm was used as substrate for the catalysts thin film in the electrochemical measurements. The thin film catalysts layer was prepared as the working electrode as follows: a mixture containing 10.0 mg catalysts, 1.9 mL ethanol and 0.1 mL Nafion solution (5.0 wt%) were dispersed in a ultrasonic bath for 15 min to obtain a well-dispersed ink. The ink was then quantitatively transferred onto the surface of GC electrode using a micropipette, and dried under an infrared lamp to obtain a catalysts thin film. The estimated catalysts loading were 0.125 mg cm^{-2} in this study. Cyclic voltammetries (CVs) were carried out in N_2-saturated 0.1 mol L^{-1} $HClO_4$ aqueous solutions with the scan rate of 50 mV s^{-1}. The accelerated durability tests (ADT) were conducted by CVs method between 0 to 1.1 V with the scan rate of 100 mV s^{-1} in N_2-saturated 0.1 mol L^{-1} $HClO_4$ aqueous solutions. For oxygen reduction experiment, the rotating disk electrode (RDE) was carried out in an O_2-saturated 0.1 mol L^{-1} $HClO_4$ aqueous solutions scanned from 0 to 1.1 V at a rotating speed of 1600 rpm with a scan rate of 5 mV s^{-1}.

3. Results and discussion

Fig. 2 presents the XRD patterns of the prepared samples. The peaks at 37.69° (1 1 1), 43.80° (2 0 0), 63.68° (2 2 0), 76.43° (3 1 1) and 80.49° (2 2 2) indicating the characteristic diffraction peaks of polycrystalline WN (JCPDS#65-2898). The calculated crystal size according to the Scherrer formula is 19.4 nm. Meanwhile, the XRD patterns of both catalysts display the typical characteristics of a crystalline Pt face centered cubic structure (JCPDS#35-0768). The average crystal sizes for Pt on Pt-WN/CNTs-M and Pt/CNTs-M are 4.3 nm and 3.4 nm. This might be for the larger density of WN, which are easily sedimentation during the impregnation process.

In order to further investigate the particle size distribution of the prepared catalysts, TEM images of Pt-WN/CNTs-M and Pt/CNTs-M are provided in Fig. 3. As clearly displayed, the Pt particles are uniformly distributed on CNTs-M. While there are some

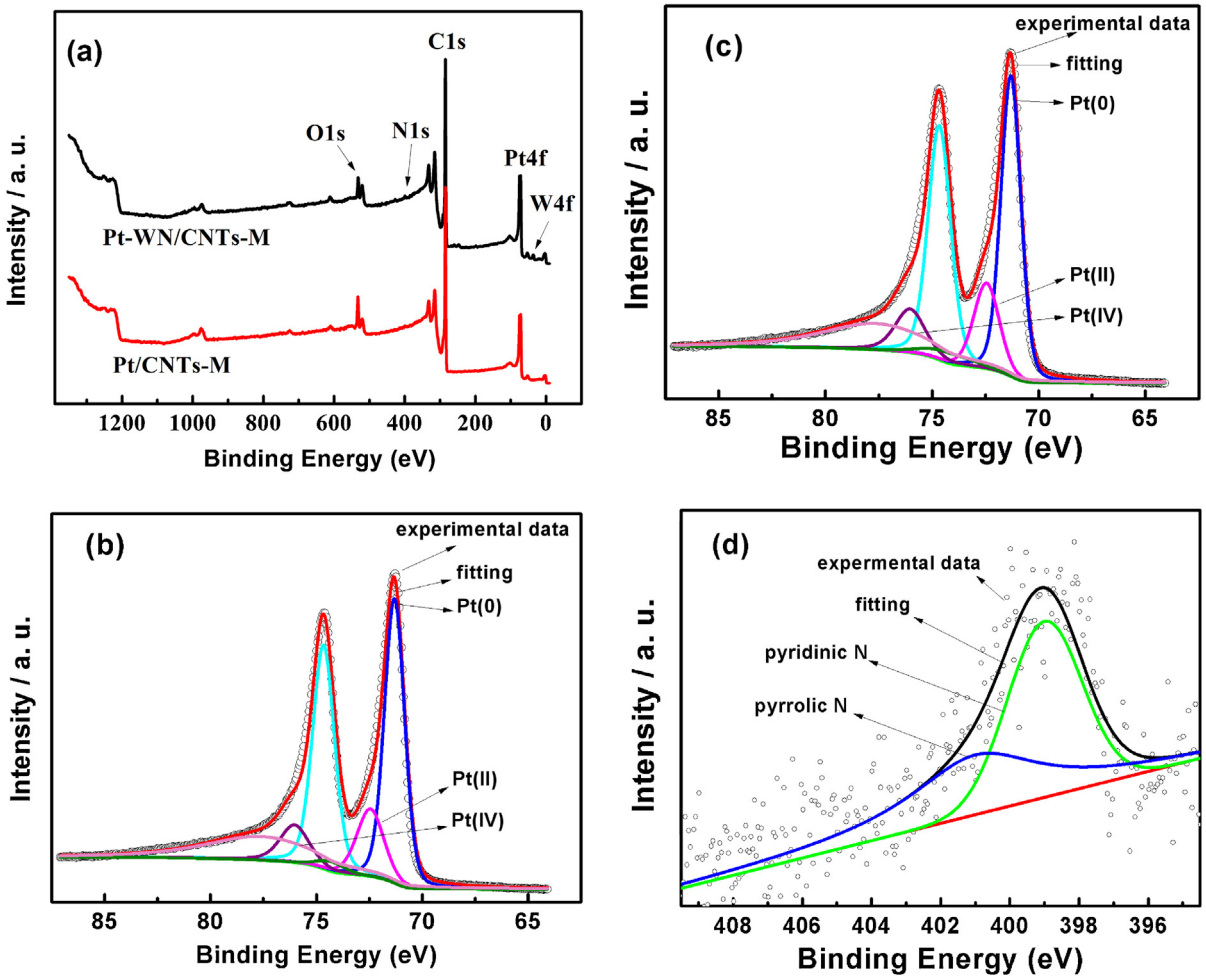

Fig. 4. (a) XPS surveys for the prepared catalysts. XPS spectrum of the Pt4f photoemission from the Pt/CNTs-M (b) and Pt-WN/CNTs-M (c). (d) XPS N1s of Pt-WN/CNTs-M.

agglomerations on the surface of WN/CNTs-M, which could be attributed for the large density of WN that are easily sedimentation during the synthesize processing as mentioned. Based on 300 particles measured in random regions, the particle size distributions are narrow and the average particle sizes for Pt on Pt-WN/CNTs-M and Pt/CNTs-M are estimated to be 4.1 nm and 3.4 nm, respectively. Meanwhile, the Pt contents that quantified by ICP-AES are 88.3% and 89.7% for Pt-WN/CNTs-M and Pt/CNTs-M. Apparently, the Pt/CNTs-M has higher Pt content than Pt-WN/CNTs-M. As mentioned above, the WN has larger density than carbon nanotubes, which are easily sedimentation during the impregnation process and cause some agglomerations. Therefore, it is relatively difficult for the reduced platinum particles absorbed on the surface of WN/CNTs-M.

The XPS measurement was also adopted to characterize the surface of the prepared catalysts. As shown in Fig. 4(a), both catalysts exhibit O1s peaks, indicating the oxidation functionalization produces some oxygen-containing functional groups on CNTs surface [32]. For Pt/CNTs-M and Pt-WN/CNTs-M, the XPS spectra are characterized by a doublet containing a binding energy (BE) of 71.4 eV (Pt $4f_{7/2}$) and 74.7 eV (Pt $4f_{5/2}$), characteristic BE of Pt(0) (Fig. 4(b) and (c)). The Pt 4f spectrum can be deconvoluted into three species with BE of 71.3–74.7, 72.5–76.0, and 74.3–77.6 eV, which correspond to Pt(0), Pt(II), and Pt(IV), respectively [32]. On the basis of the areas of Pt $4f_{7/2}$, the relatively intensity of Pt(0), Pt(II), and Pt(IV) for Pt/CNTs-M was calculated to be 53.4%, 25.4%, and 21.2%, respectively. And the relatively intensity of Pt(0), Pt(II), and Pt(IV) for Pt-WN/CNTs-M was calculated to be 53.9%, 26.0%, and 20.1%, respectively. The corresponding results of the XPS analysis of the prepared catalysts are summarized in Table 1. Obviously, there is almost no difference of the surface electronic state of Pt between Pt/CNTs-M and Pt-WN/CNTs-M. For no further heat treatment is adopted, it is hard for WN to modify the electronic state of Pt in the Pt-WN/CNTs-M catalysts [36].

While the N1s peak displayed in Pt-WN/CNTs-M are relatively lower than C1s, Pt4f and W4f, indicating low nitrogen content (1.32 at%). As we know, the nitrogen content has close relationship with reduction temperature; the higher reduction temperature usually leads to relatively higher nitrogen content [37]. In this work, the synthesizing temperature is 800 °C, which is relatively low for more nitrogen atoms doped in the hybrid. Fig. 4(d) demonstrates the high-resolution N1s spectra of Pt-WN/CNTs-M, the peaks at 401.0 eV and 389.9 eV are attributed to the pyrrolic-like (35.0%) and pyridinic-like (65%) nitrogen [28], with the pyridine nitrogen

Table 1
Distribution of Pt species in Pt-WN/CNTs-M and Pt/CNTs-M.

	Pt species	Binding energy (eV)		Rel density (%)
		Pt $4f_{7/2}$	Pt $4f_{5/2}$	
Pt/CNTs-M	Pt(0)	71.3	74.7	53.4
	Pt(II)	72.5	76.0	25.4
	Pt(IV)	74.3	77.6	21.2
Pt-WN/CNTs-M	Pt(0)	71.3	74.7	53.9
	Pt(II)	72.5	76.0	26.0
	Pt(IV)	74.3	77.6	20.1

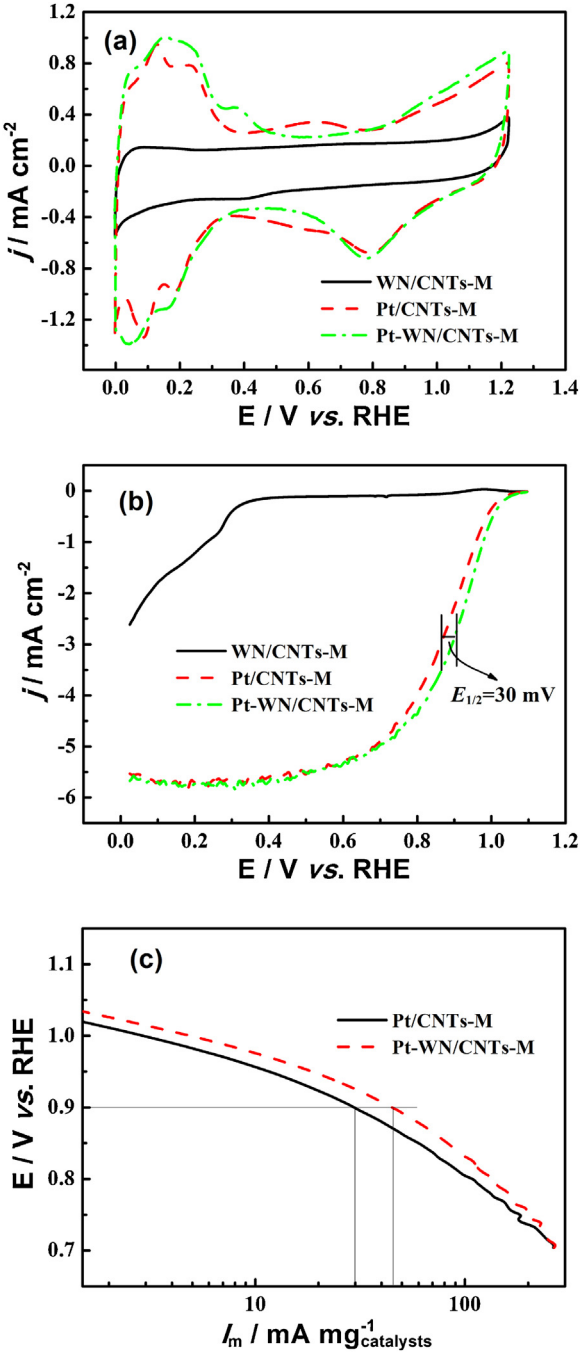

Fig. 5. (a) The CV curves for the as-prepared catalysts in N_2-purged 0.1 mol L^{-1} $HClO_4$ aqueous solutions at 25 °C, scan rate 50 mV s^{-1}. (b) ORR polarization curves for the catalysts in O_2-saturated 0.1 mol L^{-1} $HClO_4$ aqueous solutions at 25 °C, scan rate 5 mV s^{-1}, rotating rate 1600 rpm. (c) Comparison of mass activities (I_m).

being dominant. As reported [38], the pyridinic nitrogen is more activity than its pyrrolic counterpart which is favorable for oxygen reduction.

Fig. 5(a) and (b) demonstrates the CV curves of catalysts in N_2-saturated 0.1 mol L^{-1} $HClO_4$ aqueous solutions. By integrating the hydrogen desorption charges according to the CVs in Fig. 5(a), the electrochemical surface area (ESA) of catalysts can be calculated [30]. The charges, Q_H, of Pt-WN/CNTs-M and Pt/CNTs-M are 5.37 mC cm^{-2} and 4.65 mC cm^{-2}. Obviously, the Pt-WN/CNTs-M has larger ESA, which is 1.15 times larger compared to Pt/CNTs-M. This improvement can be ascribed to the intrinsic characteristics of WN/CNTs-M hybrid, which might form hydrogen tungsten bronze in Pt-WN/CNTs-M catalysts and elevate their catalytic activity [39]. Moreover, as the ORR curves displayed in Fig. 5(b), the half way potential $E_{1/2}$ of Pt-WN/CNTs-M positively shifts approximately 30 mV compared with Pt/CNTs-M, indicating the oxygen reduction process is more favorable on Pt-WN/CNTs-M than that on Pt/CNTs-M.

The kinetic current (I_K) can be calculated by using the Koutecky–Levich equation [40]:

$$\frac{1}{I} = \frac{1}{I_K} + \frac{1}{I_d} \quad (1)$$

where I is the measured current and I_d is the diffusion limited current. The mass activities for Pt-WN/CNTs-M and Pt/CNTs-M in 0.90 V showed in Fig. 5(c) are 44.67 mA mg^{-1} catalysts and 29.55 mA mg^{-1} catalysts. Obviously, the Pt-WN/CNTs-M is more active for oxygen reduction than Pt/CNTs-M. As reported, the oxidation procedure could produce quantity of oxygen-containing functional groups on CNTs surface, especially the carboxylic groups, which favor oxygen reduction [41]. In this work, the difference between Pt-WN/CNTs-M and Pt/CNTs-M is the introduction of WN nanocrystals. At the same time, the hydrogen tungsten bronze might be formed in Pt-WN/CNTs-M, which is beneficial to enhance the catalytic performance for oxygen reduction [39]. Furthermore, as discussed above, the samples that synthesized in ammonia atmosphere produce some nitrogen-contain groups on WN/CNTs-M hybrid, especially the pyridinic-like nitrogen, which could enhance the interaction between Pt metallic particles and catalyst supports and improve the catalytic activities toward oxygen reduction [28,42,43]. Therefore, the improvement of performance could be attributed to the synergistic effect between WN and Pt in the Pt-WN/CNTs-M catalysts and the nitrogen-doping effect of carbon nanotubes with ammonia.

Meanwhile, it is well known that the stability for the prepared catalysts is also significant. Therefore, the ADT was conducted and the corresponding results are shown in Fig. 6. Obviously, as Fig. 6(a) displays, the ESA of both catalysts are declining with time, which could be ascribed to agglomeration, dissolution and/or detachment of Pt particles [44,45]. While the activity of Pt-WN/CNTs-M declines more slowly than Pt/CNTs-M. The ESA of Pt-WN/CNTs-M reduces 23.66% after 4000 cycles, whereas the Pt/CNTs-M reduces 30.20%, which indicates better stability. Fig. 5(b) further presents the ORR curves of both catalysts before and after ADT. Apparently, both catalysts display good stability for oxygen reduction even after 4000 cycles, while the change on Pt-WN/CNTs-M is negligible. The decline rate D of mass activity that can be calculated as follows:

$$D = \frac{\text{initial mass activity} - \text{final mass activity}}{\text{initial mass activity}} \times 100\% \quad (2)$$

As displayed in Fig. 6(c) and (d), the initial and final mass activities for Pt-WN/CNTs-M at 0.90 V are 44.67 mA mg^{-1} catalysts and 42.43 mA mg^{-1} catalysts, which decrease 5.01%. While the initial and final mass activities for Pt/CNTs-M at 0.90 V are 29.55 mA mg^{-1} catalysts and 24.89 mA mg^{-1} catalysts, which decreases 15.77%. It means that the Pt-WN/CNTs-M catalysts are much more stable than Pt/CNTs-M. As reported [33], the CNTs have good corrosion resistance in acid and basic solutions in electrochemical environments due to their relatively high graphitic degrees. And the HF etching procedure could produce some micropores on CNTs surface, which could enlarge the contact area between Pt metallic particles and supports and improve the stability of catalysts [31]. Meanwhile, the further modification by H_2SO_4/HNO_3 solutions could produce some oxygen-contain functional groups on the surface of CNTs, which could efficiently improve their hydrophily and enhance the interactions between Pt metallic particles and CNTs [32]. These procedures are benefited for enhancing the catalytic activity for

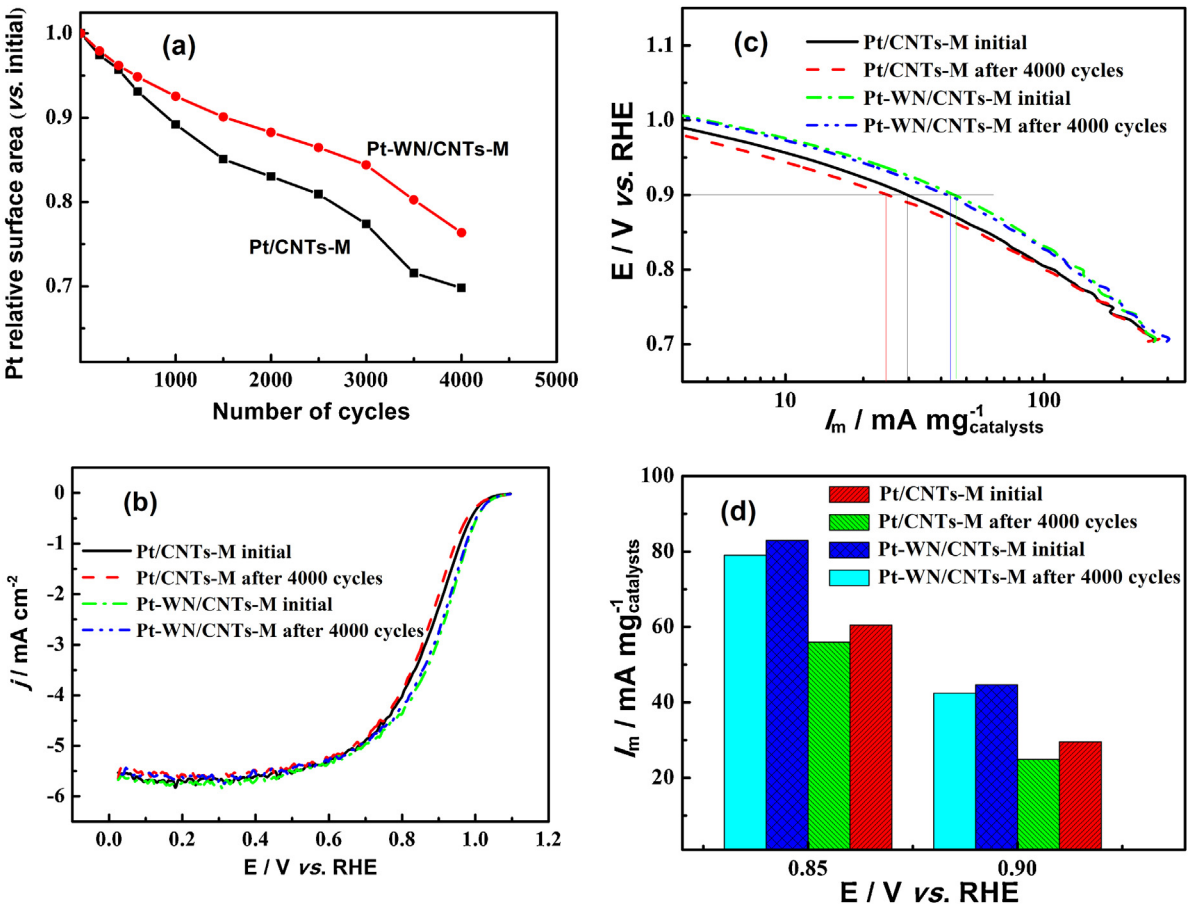

Fig. 6. (a) ESA as a function of the number of CV cycles for different catalysts in N_2-purged 0.1 mol L^{-1} $HClO_4$ aqueous solutions. (b) ORR polarization curves for the catalysts in O_2-saturated 0.1 mol L^{-1} $HClO_4$ aqueous solutions before and after ADT, 25 °C, scan rate 5 mV s^{-1}, rotating rate 1600 rpm. (c) Comparison of mass activities (I_m) before and after cycling. (d) Comparison of mass activities for Pt-WN/CNTs-M and Pt/CNTs-M before and after cycling at 0.85 V and 0.90 V.

oxygen reduction and improving the stability of catalysts. Therefore, both catalysts display good stability in ADT. In this work, the CNTs employed as catalyst supports are first etched by HF solutions, and subsequently modified by H_2SO_4/HNO_3 solutions. The sole difference between Pt-WN/CNTs-M and Pt/CNTs-M is the introduction of WN nanocrystals, which are employed to decorate carbon nanotubes and the corresponding hybrid is adopted as catalyst supports. Consequently, we believe that such high activity for oxygen reduction and stability in acid solutions predominantly origins from the synergistic effect between WN and Pt in the Pt-WN/CNTs-M catalysts, which could form hydrogen tungsten bronze and improve the performance for oxygen reduction [39]. Meanwhile, the WN/CNTs-M hybrid that synthesized in ammonia atmosphere produces some nitrogen-containing functional groups which could also reinforce the interactions between Pt particles and supports and improve the catalytic performance for oxygen reduction reaction.

4. Conclusions

In this work, the fabrication and performance of WN/CNTs-M hybrid supported Pt catalysts for oxygen reduction reaction are investigated for the first time. The results display that the prepared Pt-WN/CNTs-M catalysts demonstrate significantly improved performance toward oxygen reduction in acid solutions in comparison with Pt/CNTs-M catalysts. The reason could be predominantly attributed to the synergistic effect between tungsten nitride and Pt in the Pt-WN/CNTs-M catalysts and the nitrogen-doping effects of carbon nanotubes by ammonia. The tungsten nitride decorated carbon nanotubes hybrid might be a promising alternative for low-Pt or non-Pt catalysts for the commonly used Pt/C catalysts, which might be a cost-effective and reliable cathode catalyst for proton exchange membrane fuel cells.

Acknowledgments

The authors gratefully acknowledge the financially support by the Fundamental Research Funds for the Central Universities (2013QNA48).

References

[1] X.M. Ma, H. Meng, M. Cai, P.K. Shen, Journal of the American Chemical Society 134 (2012) 1954–1957.
[2] Z.H. Wen, S.Q. Ci, F. Zhang, X.L. Feng, S.M. Cui, S. Mao, S.L. Luo, Z. He, J.H. Chen, Advanced Materials 24 (2012) 1399–1404.
[3] J. Greeley, I.E.L. Stephens, A.S. Bondarenko, T.P. Johansson, H.A. Hansen, T.F. Jaramillo, J. Rossmeisl, I. Chorkendorff, J.K. Norskov, Nature Chemistry 1 (2009) 552–556.
[4] B. Genorio, R. Subbaraman, D. Strmcnik, D. Tripkovic, V.R. Stamenkovic, N.M. Markovic, Angewandte Chemie International Edition 50 (2011) 5468–5472.
[5] Y.Y. Liang, Y.G. Li, H.L. Wang, J.G. Zhou, J. Wang, T. Regier, H.J. Dai, Nature Materials 10 (2011) 780–786.
[6] D.L. Wang, H.L. Xin, Y.C. Yu, H.S. Wang, E. Rus, D.A. Muller, H.D. Abruña, Journal of the American Chemical Society 132 (2010) 17664–17666.
[7] Z.W. Chen, D. Higgins, A.P. Yu, L. Zhang, J.J. Zhang, Energy & Environmental Science 4 (2011) 3167–3192.
[8] G. Wu, K.L. More, C.M. Johnston, P. Zelenay, Science 332 (2011) 443–447.
[9] D.P. He, Y.L. Jiang, H.F. Lv, M. Pan, S.C. Mu, Applied Catalysis B—Environmental 132 (2013) 379–388.

[10] S.J. Guo, D.G. Li, H.Y. Zhu, S. Zhang, N.M. Markovic, V.R. Stamenkovic, S.H. Sun, Angewandte Chemie International Edition 52 (2013) 3465–3468.
[11] Z.X. Yan, J.M. Xie, J.J. Jing, M.M. Zhang, W. Wei, S.B. Yin, International Journal of Hydrogen Energy 37 (2012) 15948–15955.
[12] Z.X. Yan, W. Wei, J.M. Xie, S.C. Meng, X. Lu, J.J. Zhu, Journal of Power Sources 222 (2013) 218–224.
[13] S.B. Yin, M. Cai, C.X. Wang, P.K. Shen, Energy & Environmental Science 4 (2011) 558–563.
[14] Z.X. Wu, Y.X. Yang, D. Gu, Q. Li, D. Feng, Z.X. Chen, B. Tu, P.A. Webley, D.Y. Zhao, Small 5 (2009) 2738–2749.
[15] Z.X. Yan, G.Q. He, M. Cai, H. Meng, P.K. Shen, Journal of Power Sources 242 (2013) 817–823.
[16] Z.X. Yan, M. Cai, P.K. Shen, Scientific Reports 3 (2013), http://dx.doi.org/10.1038/srep01646.
[17] P.K. Shen, S.B. Yin, Z.H. Li, C. Chen, Electrochimica Acta 55 (2010) 7969–7974.
[18] I.J. Hsu, Y.C. Kimmel, Y. Dai, S.L. Chen, J.G.G. Chen, Journal of Power Sources 199 (2012) 46–52.
[19] Y. Wang, S.Q. Song, V. Maragou, P.K. Shen, P. Tsiakaras, Applied Catalysis B—Environmental 89 (2009) 223–228.
[20] C.H. Liang, L. Ding, C.A. Li, M. Pang, D.S. Su, W.Z. Li, Y.M. Wang, Energy & Environmental Science 3 (2010) 1121–1127.
[21] D.J. Ham, J.S. Lee, Energies 2 (2009) 873–899.
[22] F. Mazza, S. Trassatti, Journal of the Electrochemical Society 110 (1963) 847–849.
[23] H.X. Zhong, H.M. Zhang, G. Liu, Y.M. Liang, J.W. Hu, B.L. Yi, Electrochemistry Communications 8 (2006) 707–712.
[24] Z.B.Z. Wei, P. Grange, B. Delmon, Applied Surface Science 135 (1998) 107–114.
[25] T. Ando, S. Izhar, H. Tominaga, M. Nagai, Electrochimica Acta 55 (2010) 2614–2621.
[26] H. Tominaga, M. Nagai, Electrochimica Acta 54 (2009) 6732–6739.
[27] S.B. Yin, L.X. Yang, L. Luo, F. Huang, Y.H. Qiang, H.W. Zhang, Z.X. Yan, New Journal of Chemistry (2013), http://dx.doi.org/10.1039/C3NJ00717K.
[28] D.S. Yu, Q.A. Zhang, L.M. Dai, Journal of the American Chemical Society 132 (2010) 15127–15129.
[29] W.C. Sheng, S.W. Lee, E.J. Crumlin, S. Chen, Y. Shao-Horn, Journal of the Electrochemical Society 158 (2011) B1398–B1404.
[30] S.B. Yin, P.K. Shen, S.Q. Song, S.P. Jiang, Electrochimica Acta 54 (2009) 6954–6958.
[31] F.P. Hu, P.K. Shen, Y.L. Li, J.Y. Liang, J. Wu, Q.L. Bao, C.M. Li, Z.D. Wei, Fuel Cells 8 (2008) 429–435.
[32] Z.Q. Tian, S.P. Jiang, Y.M. Liang, P.K. Shen, Journal of Physical Chemistry B 110 (2006) 5343–5350.
[33] S.B. Yin, L. Luo, C. Xu, Y.L. Zhao, Y.H. Qiang, S.C. Mu, Journal of Power Sources 198 (2012) 1–6.
[34] S.H. Sun, D.Q. Yang, D. Villers, G.X. Zhang, E. Sacher, J.P. Dodelet, Advanced Materials 20 (2008) 571–574.
[35] A.L. Patterson, Physical Review 56 (1939) 978–982.
[36] C. Kok Poh, S. Hua Lim, Z. Tian, L. Lai, Y. Ping Feng, Z. Shen, J. Lin, Nano Energy 2 (2013) 28–39.
[37] H. Meng, N. Larouche, M. Lefevre, F. Jaouen, B. Stansfield, J.P. Dodelet, Electrochimica Acta 55 (2010) 6450–6461.
[38] S. Kundu, T.C. Nagaiah, W. Xia, Y. Wang, S.V. Dommele, J.H. Bitter, M. Santa, G. Grundmeier, M. Bron, W. Schuhmann, M. Muhler, The Journal of Physical Chemistry C 113 (2009) 14302–14310.
[39] Z.H. Zhang, X.G. Wang, Z.M. Cui, C.P. Liu, T.H. Lu, W. Xing, Journal of Power Sources 185 (2008) 941–945.
[40] D.L. Wang, H.L.L. Xin, R. Hovden, H.S. Wang, Y.C. Yu, D.A. Muller, F.J. DiSalvo, H.D. Abruña, Nature Materials 12 (2013) 81–87.
[41] S. Zhang, Y.Y. Shao, Y.Z. Gao, G.Y. Chen, Y.H. Lin, G.P. Yin, Journal of Power Sources 196 (2011) 9955–9960.
[42] Y.G. Chen, J.J. Wang, H. Liu, M.N. Banis, R.Y. Li, X.L. Sun, T.K. Sham, S.Y. Ye, S. Knights, Journal of Physical Chemistry C 115 (2011) 3769–3776.
[43] Z.M. Sheng, C.X. Guo, C.M. Li, Electrochemistry Communications 19 (2012) 77–80.
[44] R.M. Darling, J.P. Meyers, Journal of the Electrochemical Society 150 (2003) A1523–A1527.
[45] G. Zhang, Z.G. Shao, W.T. Lu, F. Xie, H. Xiao, X.P. Qin, B.L. Yi, Applied Catalysis B–Environmental 132 (2013) 183–194.